Elegant design of electrode and electrode/electrolyte interface in lithium-ion batteries by atomic layer deposition

2015 Nanotechnology 26 024001

(http://iopscience.iop.org/0957-4484/26/2/024001)

IOP Publishing Nanotechnology
Nanotechnology 26 (2015) 024001 (14pp) doi:10.1088/0957-4484/26/2/024001

Review

Elegant design of electrode and electrode/electrolyte interface in lithium-ion batteries by atomic layer deposition

Jian Liu and Xueliang Sun[1]

Department of Mechanical and Materials Engineering, University of Western Ontario, London, ON, Canada, N6A 5B9

E-mail: xsun@eng.uwo.ca

Received 4 July 2014, revised 7 August 2014
Accepted for publication 15 August 2014
Published 16 December 2014

Abstract

Lithium-ion batteries (LIBs) are very promising power supply systems for a variety of applications, such as electric vehicles, plug-in hybrid electric vehicles, grid energy storage, and microelectronics. However, to realize these practical applications, many challenges need to be addressed in LIBs, such as power and energy density, cycling lifetime, safety, and cost. Atomic layer deposition (ALD) is emerging as a powerful technique for solving these problems due to its exclusive advantages over other film deposition counterparts. In this review, we summarize the state-of-the-art progresses of employing ALD to design novel nanostructured electrode materials and solid-state electrolytes and to tailor electrode/electrolyte interface by surface coatings in order to prevent unfavorable side reactions and achieve optimal performance of the electrode. Insights into the future research and development of the ALD technique for LIB applications are also discussed. We expect that this review article will provide resourceful information to researchers in both fields of LIBs and ALD and also will stimulate more insightful studies of using ALD for the development of next-generation LIBs.

Keywords: atomic layer deposition, lithium-ion battery, surface coating, electrode material, electrode/electrolyte interface

(Some figures may appear in colour only in the online journal)

1. Introduction

At present, there is growing awareness of the necessity to develop electric vehicles (EVs) and plug-in hybrid electric vehicles (PHEVs) in order to reduce fossil fuel dependence and improve environmental stewardship. Lithium-ion batteries (LIBs) have been considered as one of the most promising energy storage systems for EVs and PHEVs because they can offer a higher operative voltage and energy density than the other available competing technologies [1, 2]. The interest in EVs and PHEVs has stimulated research in both industry and academia to develop the next generation of LIBs for EVs and PHEVs that can match the performance of internal combustion vehicles, and great advances have been made so far. For example, in 2010, General Motors introduced Chevrolet Volt EVs into the market, which can travel up to 40 miles using its LIB pack [3]. In late 2010, Nissan introduced the Leaf, a 100-mile range EV that used an advanced LIB as its only power source [3]. However, to compete with internal combustion vehicles, the PHEVs and EVs powered by LIBs should travel a 40–80 mile range and a 300–400 mile range, respectively, on a single charge [2]. Therefore, big challenges still remain for rechargeable lithium batteries in terms of energy density, cycling lifetime, safety, and cost.

[1] Author to whom any correspondence should be addressed.

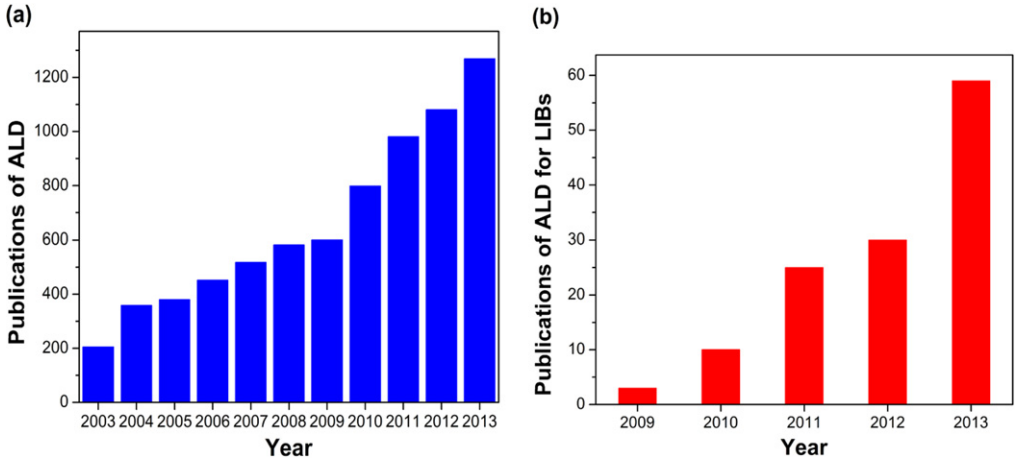

Figure 1. The number of publications on (a) ALD from 2003–2013 and (b) ALD for LIB application from 2009–2013, analysed from the Web of Science.

Since the performance of LIBs is dependent on the choice of electrode materials, it is inevitable to develop new electrode materials with highly desirable electrochemical properties such as high specific capacity, appropriate working voltages, and high cycling stability [4]. In recent years, designing nanostructured electrode materials has been a widely used and effective approach to boosting the performance of LIBs [5–7]. Nanostructured anode and cathode materials can provide many advantages for LIBs such as short path length for electron and lithium ion transport, high electrode/electrolyte contact area for fast charging and discharging, and good accommodation of strain during lithium insertion/removal [5]. A wide range of chemical and physical methods have been developed for synthesis of nanostructured materials, such as sol-gel, hydrothermal, chemical vapor deposition, and pulsed laser deposition [8]. After choosing an electrode material, surface coating is an additional step to further improve the electrochemical performance by inhibiting unfavorable phenomena from occurring in the electrode and/or at the electrode/electrolyte interface [9, 10]. Surface coating has generally been done by solution-based methods, which first involve mixing electrode materials with precursors then annealing the mixtures at elevated temperatures to form a coating layer. The post-annealing sometimes results in structural change in the active electrode materials.

Atomic layer deposition (ALD) has attracted increasing attention in the development of next-generation LIBs in recent years [11–13]. ALD is a thin film deposition technique that is based on the sequential use of self-limiting gas-solid reactions [14–16]. Different from other film deposition methods, such as chemical vapor deposition and sputtering, in an ALD process the chemical source vapors are introduced into the reaction chamber alternately, one at a time, separated by complete purging with an inert gas. Each precursor exposure step saturates the surface, resulting in self-limiting film growth [14–16]. The unique reaction mechanism enables ALD many exclusive advantages: (i) extremely uniform and conformal deposition of thin films, even on high-aspect-ratio three-dimensional (3D) substrates [17]; (ii) precisely controlled film thickness at the nanoscale level; and (iii) low deposition temperatures (even down to room temperature (RT)) [14–16]. Due to these advantages, ALD has been used as a powerful technique for synthesis and surface engineering of various types of nanostructures for a wide range of applications [18–24]. The rising number of scientific publications on ALD per year, as shown in figure 1(a), testifies to the increasing world-wide interest in ALD. Two review articles published in 2012 have highlighted the importance of ALD in designing novel nanostructured electrode materials and in realizing desirable surface coatings on the electrode in LIBs [11, 12]. On the other hand, a considerable number of studies reporting the application of ALD in LIBs (figure 1(b)) justifies the necessity to review recent advances in this field—in particular, rational design of electrode and electrode/electrolyte interface for LIBs. Herein, we will summarize up-to-date applications of ALD in the fabrication of electrode materials and solid-state electrolytes and in the realization of desirable surface coatings on electrodes. Focus will be given to the most recent progresses in the above two directions. In addition, insights into the future research of ALD applications in LIBs will also be discussed at the end.

2. Fabrication of electrode materials and solid-state electrolytes by ALD

The development of electrode materials and solid-state electrolytes by ALD can be divided into two strategies. One is to design novel anode and cathode nanocomposites, which can be directly used as electrode materials in LIBs. The other is to coat electrodes and solid-state electrolyte thin films into two-dimensional (2D) and 3D substrates, with the aim of eventually fabricating 2D and 3D all-solid-state microbatteries. In particular, ALD appears the most promising method for the fabrication of 3D microbatteries, due to its great capability to coat conformal and pinhole-free films in high-aspect-ratio 3D substrates [12, 13, 25, 26]. Advances in these two approaches first require the establishment of ALD processes for target electrode materials and solid-state electrolytes. Table 1 summarizes the anode, cathode, and solid-state electrolyte

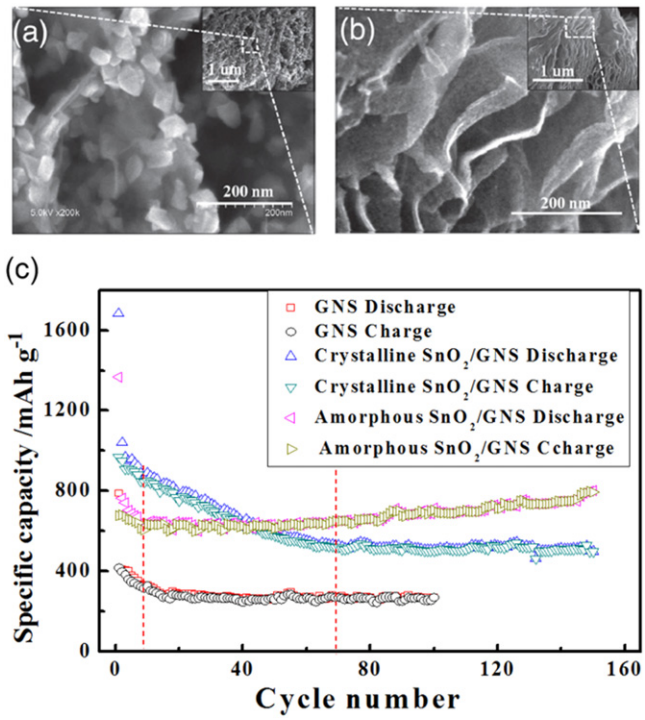

Figure 2. SEM images of (a) crystalline and (b) amorphous SnO_2/GNS; (c) cycling stability of crystalline and amorphous SnO_2/GNS in comparison with graphene. Reproduced with permission from Wiley [31].

materials that have been synthesized by ALD and demonstrated for battery applications [27–53].

2.1. Anodes by ALD

Anodes prepared by ALD are mainly transition metal oxides (TiO_2 [27–30], SnO_2 [31, 32], and Co_3O_4 [33]), partially due to their mature ALD processes. These metal oxides have high theoretical capacities (such as 790 mAh g^{-1} for SnO_2 and 890 mAh g^{-1} for Co_3O_4) but suffer from significant drawbacks that hinder their practical applications in LIBs, such as large volume change for SnO_2 and low electronic and ionic conductivities for TiO_2 [7, 54]. A widely recognized approach to overcome these disadvantages is to combine metal oxides with carbonaceous nanomaterials, including graphene and carbon nanotubes (CNTs) [7, 29, 31, 54]. From this aspect, ALD provides a non-aqueous and versatile way to prepare metal oxide/carbon nanocomposites [55]. The morphological, structural, and electrochemical properties of metal oxides can be tailored by controlling the ALD parameters (precursors, temperature) [14, 31] and the surface functionality of carbon substrates [55, 56].

One typical example is amorphous and crystalline SnO_2 deposited on graphene nanosheets (GNSs) by ALD from $SnCl_4$ and H_2O at 200°–400 °C, respectively (see figures 2(a) and (b) for their morphologies) [31]. The difference in crystallinity and morphology was believed to be due to changes in the surface functional groups and reaction mechanisms at different deposition temperatures [56]. As shown in figure 2(c), electrochemical testing indicated that amorphous SnO_2/GNS underwent a steady increase in its capacity after the first 10 cycles and achieved a discharge capacity of ~800 mAh g^{-1} after 150 cycles. For crystalline SnO_2/GNS, the capacity continuously decreased in the first 70 cycles and thereafter stabilized at ~800 mAh g^{-1}. It was argued that the isotropic nature of amorphous SnO_2 and the flexible GNS matrix could better accommodate the volume change upon cycling, thereby achieving better electrochemical performance than crystalline SnO_2/GNS [31]. This work demonstrated the flexibility of ALD in controlling morphology, crystallinity, and electrochemical performance of the anode.

Recent research has reported ALD processes for lithium titanate ($Li_4Ti_5O_{12}$) [34, 35], which is a 'zerio-strain' anode material with a flat working voltage at ~1.5 V (*vs* Li^+/Li) [54]. $Li_4Ti_5O_{12}$ was deposited at 225 °C by combining Li_2O (LiO^tBu–H_2O) and TiO_2 (TTIP–H_2O) ALD subcycles [34, 35]. The composition of $Li_4Ti_5O_{12}$ could be controlled by varying the subcycle ratio between Li_2O and TiO_2. An amorphous $Li_4Ti_5O_{12}$ film with a Li/Ti ratio of 1.5 was obtained at the as-deposited state. It became a crystalline spinel structure after annealing at temperatures between 640°–950 °C. The crystalline $Li_4Ti_5O_{12}$ was proven electrochemically active [57].

A few cases have been demonstrated the use of ALD to fabricate 3D TiO_2 electrodes on Al nanorods [27] and Ni nanowires [28]. The 3D TiO_2 electrodes exhibited dramatically increased areal capacity compared to their 2D counterparts [27, 28]. Nevertheless, the fabrication of 2D and 3D all-solid-state microbatteries by ALD is still in its early stages. Advances in this field depend highly on the development of ALD processes for all the battery components, including the anode, solid-state electrolyte, and cathode. At present, various metal oxides by ALD are available and can be directly adopted as the anode for all-solid-state microbatteries [14, 27, 28]. The focus should be given to the cathode and solid-state electrolyte, which is more challenging to be synthesized by ALD, as shown below.

2.2. Cathodes by ALD

Cathode materials prepared by ALD include non-lithiated (V_2O_5 [38–40] and $FePO_4$ [41]) and lithiated materials ($LiCoO_2$ [42], $LiMn_2O_4$ [43], and $LiFePO_4$ [44]). Crystalline V_2O_5 was readily obtained by ALD without any thermal post-treatment and from VTOP and O_3 in a temperature window of 170–185 °C [38, 39]. The V_2O_5 film grown on Au-coated stainless steel disks showed an initial specific discharge capacity of 142 mAh g^{-1} in the potential range of 2.6–4.0 V, as well as excellent rate capability and cycling stability. Amorphous $FePO_4$ was deposited by ALD using a combination of Fe(thd)-O_3 and TMP-H_2O/O_3 at temperatures between 196°–376 °C [41]. The amorphous $FePO_4$ on stainless steel exhibited exceptional cyclability and capacity close to its theoretical value (178 mAh g^{-1}) at 1C. However, the non-lithiated cathodes do not contain lithium ions, and therefore cannot be used in full cells when combined with an anode (such as metal oxides by ALD).

The focus of recent work has been the development of ALD processes for lithiated cathode materials ($LiCoO_2$ [42],

Table 1. Summary of anodes, cathodes, and solid-state electrolytes synthesized by ALD [27–53].

	Material	Substrate	Precursors	Temperature	Ref.
Anode	TiO_2	Al nanorods	TiI_4–H_2O	200 °C	27
	TiO_2	Ni nanowires	$TiCl_4$–H_2O	120 °C	28
	TiO_2	graphene	$TiCl_4$–H_2O	120 °C	29
	TiO_2	peptide	TTIP–NH_3/O_2	140 °C	30
	SnO_2	graphene	$SnCl_4$–H_2O	200, 400 °C	31
	SnO_2	SS	$Sn(O^tBu)^5$–O^- ions	200 °C	32
	Co_3O_4	TiN/Si	$CoCp_2$–plasma O_2	300 °C	33
	$Li_4Ti_5O_{12}$	NCNTs	(LiO^tBu–H_2O) + (TTIP–H_2O)	225 °C	34
	$Li_xTi_yO_z$	Si	(LiO^tBu–H_2O) + (TTIP–H_2O)	225 °C	35
	GaS_x	Si, CNTs	$Ga_2(NMe_2)_6$–H_2S	125–225 °C	36, 37
Cathode	V_2O_5	Si, SS, AAO, CNTs	VTOP–O_3	170–185 °C	38, 39
	V_2O_5	Si, glass, SS	$VO(thd)_2$–O_3	215 °C	40
	$FePO_4$	Si, glass, SS	($Fe(thd)_3$–O_3) + (TMP–H_2O/O_3)	196–376 °C	41
	$LiCoO_2$	Si/SiO_2, Si/TiO_2/Pt	($CoCp_2$–plasma O_2) + (LiO^tBu–plasma O_2)	325 °C	42
	$Li_xMn_2O_4$	Si, SS	($Mn(thd)_3$–O_3) + ($Li(thd)$–O_3)	225 °C	43
	$LiFePO_4$	Si, CNTs	5 × ($FeCp_2$–O_3–TMP–H_2O) + (LiO^tBu–H_2O)	300 °C	44
Solid-state electrolyte	$(Li,La)_xTi_yO_z$	Si, glass	($TiCl_4$–H_2O) + ($La(thd)_3$–O_3) + (LiO^tBu–H_2O)	225 °C	45
	$LiAlO_x$	Si, Teflon	(LiO^tBu–H_2O) + (TMA–H_2O)	225 °C	46, 47
	Li_3PO_4	Si, glass	LiO^tBu or LiHMDS–TMP	225–350 °C	48
	Lithium silicate	Si	LiHMDS–O_3	150–400 °C	49
	$LiTaO_3$	Si	(LiO^tBu–H_2O) + ($Ta(OEt)_5$–H_2O)	225 °C	50
	$LiNbO_3$	Si, glass	(LiHMDS–H_2O) + ($Nb(OEt)_5$–H_2O)	235 °C	51
	Li_3N	Glass, Si, Ti	LiHMDS–NH_3	167 °C	52
	$LiSiAlO_2$	Si, Ge	(TMA–H_2O) + (LiO^tBu–H_2O) + (TEOS–H_2O))	290 °C	53

Footnotes: Room temperature–RT; Trimethyl aluminum–TMA; Tetrakis(dimethylamido)zirconium (IV)–$Zr(NMe_2)_4$; Titanium isopropoxides–TTIP; Lithium tert-butoxide–LiO^tBu; Tin(IV) tert-butoxide–$Sn(O^tBu)^5$; hexakis(dimethylamido)digallium–$Ga_2(NMe_2)_6$; Vanadyl triisopropoxide–VTOP; trimethyl phosphate–TMP; lithium hexamethyldisilazide–LiHMDS; Tantalum(V) ethoxide–$Ta(OEt)_5$; tetraethyl orthosilane–TEOS; stainless steel–SS; Anodic Aluminum Oxide–AAO; Nitrogen-doped carbon nanotubes–NCNTs.

$LiMn_2O_4$ [43], and $LiFePO_4$ [44]), which has benefited from the success of the ALD process for Li_2O (or Li_2CO_3) [58]. These lithiated cathodes were deposited by combining a Li_2O subcycle with another one or two binary oxide ALD subcycles. For example, $LiCoO_2$ was grown at 325 °C from ALD subcycles of Co_3O_4 ($CoCp_2$–plasma O_2) and Li_2CO_3 (LiO^tBu–plasma O_2) in a remote plasma ALD system [42]. The $LiCoO_2$ film yielded a growth rate of ~0.06 nm/cycle when using a recipe of four cycles of Co_3O_4 for each cycle of Li_2CO_3. A crystalline $LiCoO_2$ film was obtained after annealing at 700 °C for 6 min and exhibited electrochemical activity as measured in a three-electrode setup. The oxidation and reduction peaks for $LiCoO_2$ were observed at about 3.9 V (*vs* Li^+/Li), as seen in figure 3(a). Although the capacity of ALD-deposited $LiCoO_2$ could be improved by tuning the Co/Li dose ratio, the electrochemical storage capacity was relatively lower than the theoretical value of $LiCoO_2$ (figure 3(b)). Another study reported an ALD recipe of $Li_xMn_2O_4$ using ($Mn(thd)_3$–O_3) and ($Li(thd)$–O_3) subcycles [43]. An interesting finding in this study was that ALD-MnO_2 and ALD-V_2O_5 could be transformed into $Li_xMn_2O_4$ and $Li_xV_2O_5$, respectively, by using Li(thd)-O_3 or LiO^tBu-H_2O post-treatments. Moreover, the $Li_xMn_2O_4$ obtained with 200-cycle LiO^tBu-H_2O post-treatment exhibited 230 mAh g^{-1} at 50 μA (figure 3(c)) and ~190 mAh g^{-1} at 200 μA with stable cycling performance over 550 cycles (figure 3(d)).

Great progress was made recently in the synthesis of $LiFePO_4$ by ALD as a high performance cathode for LIBs [44]. $LiFePO_4$ is a representative example of lithium transition metal phosphates ($LiMPO_4$, M = Fe, Ni, Co, Mn) and currently considered as high-power cathode material for next-generation LIBs due to its high energy density, low cost, and high safety [59, 60]. After careful tuning of the surface chemistries, amorphous $LiFePO_4$ was synthesized at 300 °C by using an ALD sequence of 5 × ($FeCp_2$–O_3–TMPO–H_2O) + 1 × (LiO^tBu–H_2O) (figure 4) [44]. The growth rate of amorphous $LiFePO_4$ was ~0.9 nm/cycle on a Si (100) substrate. Crystalline $LiFePO_4$ was obtained on CNTs after annealing at 700 °C for 5 h in Ar. The scanning electron microscope (SEM) image in figure 5(a) shows that crystalline $LiFePO_4$ covers the majority of the CNT surface. The high resolution transmission electron microscopy (HRTEM) image of crystalline $LiFePO_4$ (figure 5(b)) exhibits clear crystal planes with a d-spacing of 0.39 nm, corresponding to the (210) planes of orthorhombic $LiFePO_4$. More excitingly, the crystalline $LiFePO_4$ on CNTs exhibited high discharge capacity, excellent rate capability, and ultra-long cycling life, as displayed in figures 5(c) and (d). The crystalline $LiFePO_4$ delivered a discharge capacity of ~70 mAh g^{-1} at 60 C (corresponding to 1 min for each full charge and each discharge process) and of ~160 mAh g^{-1} at 0.1 C, which is very close to the theoretical capacity of 175 mAh g^{-1}. Furthermore, the crystalline $LiFePO_4$ had no apparent capacity degradation at 1 C even after 2000 cycles. This work paves the way toward fabrication of $LiMPO_4$ as a next-generation high-power cathode material for LIBs.

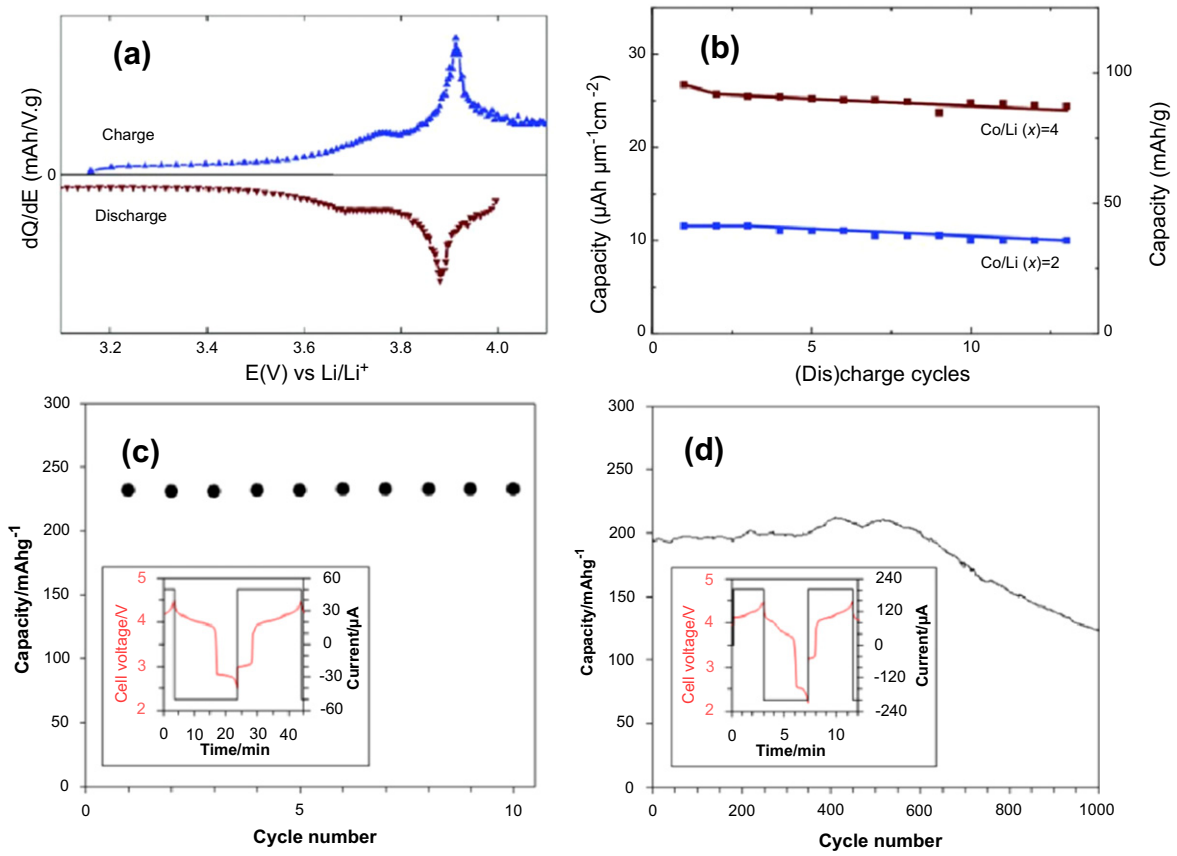

Figure 3. (a) The derivative of the storage capacity with respect to the electrode potential ($x = 4$) and (b) the electrochemical storage capacity upon cycling showing data for ALD-deposited $LiCoO_2$ when the used Co:Li dose ratio (x) was 2 and 4 [42]. (Reproduced with permission from *J. Electrochem. Soc.*, **160**, A3066 (2013). Copyright 2013, The Electrochemical Society); (c) 10 charge-discharge cycles with 50 μA and (d) 1000 charge-discharge cycles with 20 μA of an 86 nm MnO_2 film treated with 200 cycles of $LiO^tBu + H_2O$ [43]. (Adapted with permission from *J. Phys. Chem. C* **118**, 1258 (2014). Copyright 2014 American Chemical Society).

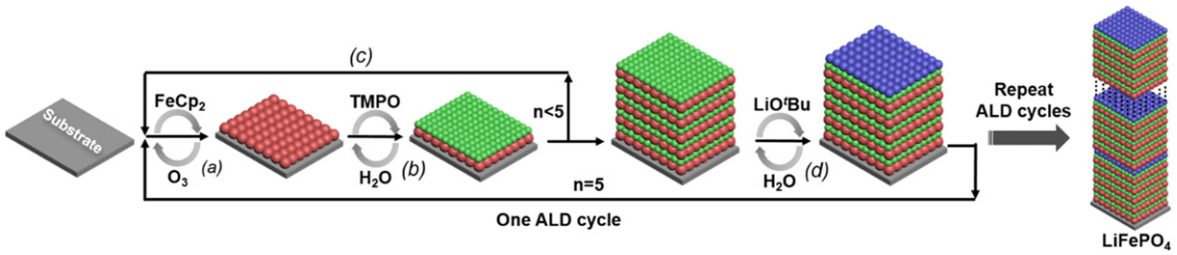

Figure 4. Atomic layer deposition of amorphous $LiFePO_4$ at 300 °C using ferrocene ($FeCp_2$), ozone (O_3), trimethylphosphate (TMPO), water (H_2O), and lithium *t*-butoxide (LiO^tBu). (a) Sequential pulse of $FeCp_2$ and O_3 leading to the growth of a Fe_2O_3 layer (red); (b) sequential pulse of TMPO and H_2O leading to deposition of a PO_x layer (green); (c) steps (a) and (b) are repeated five times; (d) sequential pulse of LiO^tBu and H_2O leading to formation of Li_2O layer (blue). One ALD cycle for the growth of amorphous $LiFePO_4$ consists of steps (a)–(d) [44].—Reproduced with permission from Wiley.

2.3. Solid-state electrolytes by ALD

Recent studies have reported the fabrication of glass-type solid-state electrolytes by ALD, as seen in table 1. Other than lithium silicate and Li_3N, the solid-state electrolytes were prepared by ALD using the sub-cycle strategy as also employed in lithiated cathode materials. For example, $LiTaO_3$ was deposited at 225 °C from Li_2O (LiO^tBu–H_2O) and Ta_2O_5 ($Ta(OEt)_5$–H_2O) with a tunable Li/Ta ratio by changing the subcycle ratio of Li_2O to Ta_2O_5 [50]. $LiAlO_2$ has been grown from Li_2O (LiO^tBu–H_2O) and Al_2O_3 (TMA–H_2O) [46, 47], while lithium silicate and Li_3N were produced by ALD using LiHMDS coupled with O_3 [49] or NH_3 [52]. A more complicated process was demonstrated for $(Li,La)_xTi_yO_z$, which was deposited by combining TiO_2 ($TiCl_4$–H_2O), La_2O_5 (La $(thd)_3$–O_3), and Li_2O (LiO^tBu–H_2O), but no ionic conductivity was reported for this solid-state electrolyte [45]. The ionic conductivities of $LiTaO_3$, $LiAlO_2$, and $LiSiAlO_2$ prepared by ALD are compared in figure 6. The highest ionic conductivity reported in the glassy solid-state electrolytes was

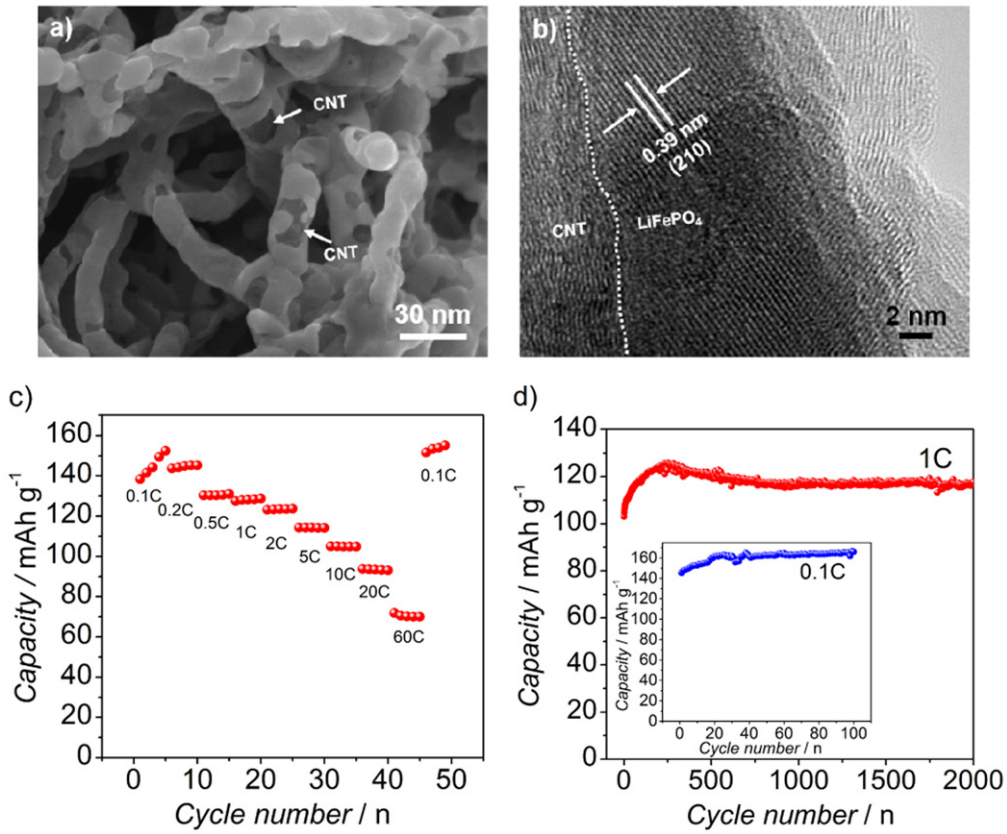

Figure 5. (a) SEM image, (b) HRTEM image, (c) rate capability, and (d) cycling stability of the annealed $LiFePO_4$/CNTs [44].—Reproduced with permission from Wiley.

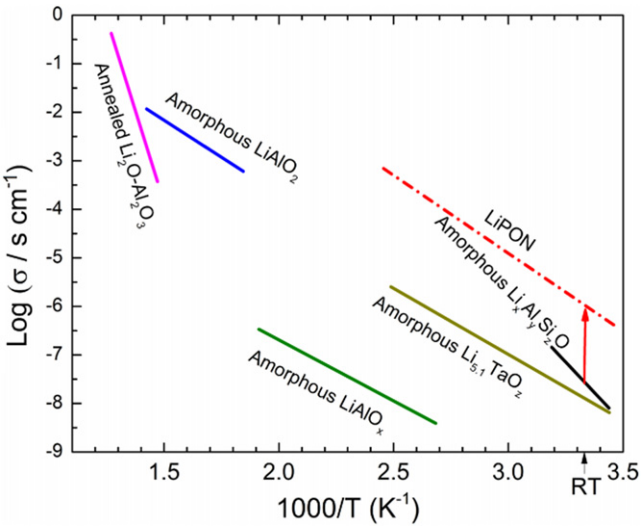

Figure 6. Ionic conductivities of solid-state electrolytes prepared by ALD [46, 50, 53, 62], in comparison with the commonly used LiPON solid-state electrolyte in thin film batteries [61].

in the order of $\sim 10^{-8}$ s cm^{-1} ($LiTaO_3$ [50] and $LiSiAlO_2$ [53]), which, however, is still relatively lower than that of LiPON (a commonly used solid-state electrolyte in thin film batteries) [61]. Nevertheless, a great advantage of ALD is the ability to prepare solid-state electrolytes in ultra-thin films to reduce internal resistance and overall battery impedance. Recent work has shown that 10 nm $LiSiAlO_2$ solid-state electrolytes prepared by ALD still functioned during the ionic-conductivity measurement [53]. Therefore, ALD is expected to play an important role in preparing ultrathin and functional solid-state electrolytes for 2D and 3D all-solid-state microbatteries.

3. Towards engineered electrode/electrolyte interfaces by ALD

Interfacial reactions always occur between the electrode and liquid electrolyte in LIBs. On one hand, the interfacial reactions are beneficial to the battery's performance when they are designable and controllable. For example, the solid electrolyte interphase (SEI) formed on the anode is critical for stabilizing the cycling performance and improving battery safety by preventing further decomposition of aqueous electrolytes. On the other hand, interfacial reactions might lead to unfavorable phenomena that can compromise the overall performance of LIBs. For instance, the SEI on the anode can consume lithium ions permanently, leading to reduced columbic efficiency of batteries [63]. For the cathode, HF generated in the electrolytes during cycling tends to dissolve the components of the cathode materials, resulting in rapid degradation of battery performance [9].

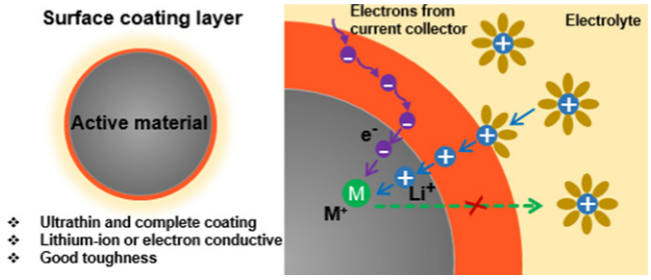

Figure 7. Schematic diagram of an ideal surface coating layer on the active materials. The surface coating should meet one or more of the following requirements: (i) ultrathin and complete coating; (ii) lithium-ion or electron conductivity; and (iii) good toughness.

Surface coating has proven an effective approach to alleviate these unwanted side reactions and thus improve the capacity retention, rate capability, and even thermal stability of electrode materials [9, 10, 64]. Ideally, the surface coating layer should meet one or more of the following requirements in order to achieve the optimal performance of electrode materials (figure 7): (i) ultrathin and complete coating. It is critical to fully protect the electrode while avoiding blocking the diffusion of lithium ions and electrons through the coating layer. Ultrathin coatings would help minimize the weight of the coating layer in the electrode, which does not contribute to the capacity; (ii) lithium-ion or electron conductivity (depending on the nature of electrodes) in order to facilitate the transport of lithium ions or electrons into/out of the electrode materials; and (iii) good toughness, in order to prevent the pulverization of electrode materials resulting from large volume change upon cycling. Surface coatings prepared by solution-based methods have been widely employed in LIBs [9, 10, 64]. In general, these methods involve first mixing the electrode materials with precursors then annealing the mixtures at elevated temperatures to form the desired coating material on the electrode surface. However, it is hard to get good control over the uniformity and thickness of the coating layer on the electrode material [64].

Due to its unique reaction mechanism, ALD provides an excellent solution to achieve uniform surface coatings with precisely tuned thickness on the electrode surface. Since 2010, surface ALD coatings have been extensively used to improve the performance of the anode and cathode. Tables 2 and 3 summarize ALD surface coatings on the anode [65–80] and cathode [62, 81–99], respectively. It can be seen that the performance of the anode and cathode was enhanced by ALD surface coating layers (mainly metal oxides) with thicknesses from a few angstroms to nanometers. It has also been shown that ALD surface coatings should be performed directly on the electrode, rather than electrode powders, in order to retain an electronically conductive network among the active material, carbon additive, and current collector [65, 77, 81, 82, 86, 91]. The direct coatings of metal oxides on the electrode benefit from the advantages of ALD, i.e., low deposition temperature and uniform deposition in porous substrates. The ALD surface coating process is quick (takes only a few minutes), non-destructive to the electrode, and easy to scale up for industry-level applications.

3.1. ALD surface coatings on the anode

ALD surface coatings on the anode mainly deal with the problems resulting from the SEI due to the decomposition products of liquid electrolytes on the anode surface. On one hand, the SEI is essential to the longevity of the battery, as it passivates the electrode surface and prevents uncontrolled decomposition of electrolytes that could lead to safety issues. On the other hand, SEI consumes Li in a battery and contributes to irreversible capacity loss, which results in reduced specific capacity and low columbic efficiency. The problem resulting from SEI formation becomes more serious in anodes that undergo large volume changes during the cycling process (such as Si, Sn, and SnO_2). During each cycle, the considerable volume change can break the anode and expose fresh electrode surfaces, where the formation of a new SEI occurs.

The ALD surface coatings serve as an artificial layer to reduce SEI formation on the surface of the anode (such as graphite [65–67] and $Li_4Ti_5O_{12}$ [73–75]), thereby improving the specific capacity, rate capability, columbic efficiency, and thermal stability. For graphite anodes, ALD of Al_2O_3 [65–67] and TiO_2 [66, 67] surface coatings with thicknesses of 0.55–5 nm have been reported to effectively suppress SEI formation at ~0.7 V (*vs* Li^+/Li), thus reducing the irreversible capacity loss and improving the specific capacity and cycling stability. Thermal analysis revealed that ALD-Al_2O_3 coating, as an 'artificial' SEI layer, was more stable than the organic SEI on graphite at high working temperatures [65]. This result suggests the prospect of using ALD metal oxide coatings on the anode to improve the battery safety. For $Li_4Ti_5O_{12}$ anodes, ultrathin ALD Al_2O_3 [75] or ZrO_2 [74] coatings (1–2 nm thick) were found to improve the specific capacity, rate capability, and columbic efficiency in an extended voltage range (0.1–2.5 V). For both graphite and $Li_4Ti_5O_{12}$, electrochemical impedance spectroscopy (EIS) analysis revealed greatly decreased resistance across the SEI layer by using ultrathin Al_2O_3, ZrO_2, and TiO_2 coatings, implying suppressed SEI formation on the anode. Visible evidence was provided by using an *in situ* scanning ion conductance microscopy (SICM) technique on MnO electrodes with and without an ALD Al_2O_3 coating (figure 8) [80]. After lithiation to 0 V, the uncoated MnO had many protrusions and increased surface roughness due to the formation of SEI, while 9 Å (10-cycle) Al_2O_3-coated MnO showed fewer protrusions and unaffected surface roughness. The difference between bare MnO and Al_2O_3-coated MnO proved that an ultrathin ALD Al_2O_3 coating alleviated the growth of SEI on the anode surface.

ALD surface coatings can reduce the serious pulverization of anode materials that undergo large volume changes upon cycling (including Si [68–72], SnO_2 [77], ZnO [78], Fe_3O_4 [79], and MnO [80]), thus improving their cycling stability. To this end, ALD surface coating materials should have good toughness along with the other desirable properties

Table 2 Summary of ALD surface coatings on the anode [65–80].

Electrode material	Coating material	ALD precursors	ALD temperature	Optimal thickness and ALD cycles	Ref
graphite	Al_2O_3	TMA–H_2O	180 °C	~0.5 nm, 5 cycles	65
graphite	TiO_2	$TiCl_4$–H_2O	RT	32–40 nm, 400 cycles	66
graphite	Al_2O_3	TMA–H_2O	<150 °C	4–5 nm, 10 cycles	67
	TiO_2	TiI_4–H_2O	<150 °C	3 nm, 10 cycles	
Patterned Si	Al_2O_3	TMA–H_2O	250 °C	~2 nm, 20 cycles	68
Si film	Al_2O_3	TMA–H_2O	N/A	~5 nm, 50 cycles	69
Si nanowires	TiN	$TiCl_4$–N_2	120 °C	5 nm, 25 cycles	70
	TiO_2	TTIP–O_2	200°, 300 °C	10 nm, 196 cycles at 200 °C	71
Si nanotubes	TiO_2	TTIP–O_2	200 °C	3 nm, N/A	72
	TiN	$TiCl_4$–N_2		3 nm, N/A	
	Al_2O_3	TMA–O_2		3 nm, N/A	
$Li_4Ti_5O_{12}$	TiN	$TiCl_4$–NH_3	500 °C	~5.8 nm, 200 cycles	73
$Li_4Ti_5O_{12}$	ZrO_2	$Zr(NMe_2)_4$–H_2O	100 °C	~1 nm, 5 cycles	74
$Li_4Ti_5O_{12}$	Al_2O_3	TMA–H_2O	N/A	~2.2 nm, 20 cycles	75
MoO_3	Al_2O_3	TMA–H_2O	180 °C	~4.4 Å, 4 cycles	76
SnO_2	Al_2O_3	TMA–H_2O	100 °C	depends on the size of SnO_2	77
ZnO	TiO_2	$TiCl_4$–H_2O	500 °C	~11 nm, 200 cycles	78
Fe_3O_4/carbon foam	Al_2O_3	TMA–H_2O	180 °C	~0.2 nm, 2 cycles	79
MnO	Al_2O_3	TMA–H_2O	150 °C	0.9 nm, 10 cycles	80

Footnote: Tetrakis(dimethylamido)zirconium (IV)–$Zr(NMe_2)_4$; Zirconium tert-butoxide–ZTB; Diethylzinc–DEZ; Not available—N/A.

(figure 7) in order to better accommodate volume expansion and contraction during cycling. The cyclic improvement by ALD surface coatings is quite obvious for this type of anode material and highly dependent on the coating material, coating thickness, and anode particle size. For example, Mitlin and co-workers compared the influence of TiO_2, TiN, and Al_2O_3 ALD coatings on the performance of Si nanotubes and found that TiO_2-coated Si nanotubes exhibited the best performance [72]. Furthermore, they disclosed that Si nanotubes with both inner and external surfaces coated with a 1.5 nm TiO_2 layer showed better performance than those with only one surface coated with 3 nm of TiO_2. Sun *et al* reported that the coating thickness to achieve optimal performance in SnO_2 anodes varied with the size of SnO_2 nanoparticles [77]. In this work, SnO_2 nanoparticles with three diameters (3 nm, 10 nm, and 25 nm) were chosen as model anodes, and ALD Al_2O_3 from TMA and H_2O was used as the coating layer. Electrochemical testing indicated that for 3, 10, and 25 nm SnO_2 nanoparticles, the optimized Al_2O_3 coating was deposited using 2, 5, and 20 ALD cycles, respectively. Besides cycling lifetime, columbic efficiency is greatly improved in this group of anode materials by ALD surface coatings [68–72, 76, 77]. In fact, the enhanced columbic efficiency is attributed to the reduced cracking of the anode, which avoids the generation of fresh anode surfaces and thus SEI formation during each cycle.

3.2. ALD surface coatings on the cathode

ALD surface coatings on the cathode are mainly dealing with problems resulting from dissolution of cathode elements into the electrolyte solution and thus aim to prolong the lifetime of the battery. ALD metal oxide coatings have been shown to improve the cycling stability and energy density of $LiCoO_2$ [81–86], $LiMn_2O_4$ [87–90], and high-voltage Mn-containing cathode materials [62, 91–98].

$LiCoO_2$ has been a dominating cathode material in commercial LIBs because of its high theoretical capacity (274 mAh g^{-1}), good rate capability, and safety. However, if more than half of the lithium ions (Li_xCoO_2, $x<0.5$) are extracted at voltages above 4.2 V, Co^{4+} will dissolve into the electrolyte, resulting in structural changes to $LiCoO_2$ and finally performance deterioration [84]. Thus, preventing the dissolution of Co^{4+} at high voltages becomes the key to making full use of the theoretical capacity of $LiCoO_2$. So far, ultrathin Al_2O_3 [81–86], TiO_2 [84, 86], and ZrO_2 [86] coatings (<1 nm in thickness) by ALD have been found to effectively protect Co^{4+} from dissolution into electrolytes. For example, two-cycle Al_2O_3 coated nano-$LiCoO_2$ delivered a discharge capacity of 133 mAh g^{-1} between 3.3–4.5 V (*vs* Li^+/Li) at a current density of 1400 mA g^{-1}, which corresponded to a 250% improvement in reversible capacity compared to bare nano-$LiCoO_2$ [82]. The improvement by the Al_2O_3 surface coating was more profound in nano-$LiCoO_2$ than in micro-$LiCoO_2$ [81, 82]. This was due to the increased dissolution of Co^{4+} from nano-$LiCoO_2$ compared to micro-$LiCoO_2$, owing to greater contact area with the electrolyte [82]. Therefore, ALD surface coatings are critical for avoiding unwanted side reactions in nanostructured cathode materials and achieving the highest possible battery performance. In comparisons of Al_2O_3, TiO_2, and ZrO_2 coatings, ALD Al_2O_3 coated $LiCoO_2$ showed the best cycling stability and capacity retention, while ALD ZrO_2 coated $LiCoO_2$ exhibited the best rate capability, especially at high current densities [86]. This result suggests that ALD metal oxide coatings functioned specifically in enhancing the performance of $LiCoO_2$. Therefore, it is possible that hybrid coatings (such as Al_2O_3/ZrO_2 and Al_2O_3/ZrO_2/Al_2O_3) would work better

Table 3 Summary of ALD surface coatings on the cathode [62, 81–99].

Electrode material	Coating material	ALD precursors	ALD temperature	Optimal thickness and ALD cycles	Ref.
$LiCoO_2$	Al_2O_3	TMA–H_2O	180 °C	~0.2 nm, 2 cycles	81
	ZnO	DEZ–H_2O	180 °C	~0.8 nm, 4 cycles	
Nano-$LiCoO_2$	Al_2O_3	TMA–H_2O	180 °C	~0.2 nm, 2 cycles	82
$LiCoO_2$	Al_2O_3	TMA–H_2O	180 °C	~0.2 nm, 2 cycles	83
$LiCoO_2$	Al_2O_3	TMA–H_2O	120 °C	N/A, 10 cycles	84, 85
	TiO_2	TTIP–H_2O	120 °C	N/A, 50 cycles	
$LiCoO_2$	Al_2O_3	TMA–H_2O	150 °C	~0.2 nm, 2 cycles	86
	TiO_2	TTIP–H_2O	85 °C	~0.3 nm, 2 cycles	
	ZrO_2	$Zr(NMe_2)_4$–H_2O	100 °C	~0.3 nm, 2 cycles	
$LiMn_2O_4$	Al_2O_3	TMA–H_2O	120 °C	~0.9 nm, 6 cycles	87, 88
$LiMn_2O_4$	ZrO_2	ZTB–H_2O	120 °C	~1.7 nm, 6 cycles	89, 90
$Li[Li_{0.20}Mn_{0.54}Ni_{0.13}Co_{0.13}]O_2$	Al_2O_3	TMA–H_2O	180 °C	N/A, 6 cycles	91
$LiNi_{1/3}Mn_{1/3}Co_{1/3}O_2$	Al_2O_3	TMA–H_2O	N/A	~0.2 nm, 2 cycles	92
$LiNi_{1/3}Mn_{1/3}Co_{1/3}O_2$	$Li_{5.1}TaO_z$	(LiO^tBu–H_2O) + 5 × ($Ta(OEt)_5$–H_2O)	225 °C	vary with testing voltage	93
$LiMn_{1.5}Ni_{0.5}O_4^{\#}$	Al_2O_3	TMA–H_2O	N/A	5 nm on anode, 50 cycles	94
$Li_{1.2}Ni_{0.15}Mn_{0.55}Co_{0.1}O_2^{\#}$	Al_2O_3	TMA–H_2O	80 °C	3.4 nm, 33 cycles	95
$Li_{1.2}Ni_{0.13}Mn_{0.54}Co_{0.13}O_2$	Al_2O_3	TMA–H_2O	150 °C	2-3 nm, 10 cycles	96
	TiO_2	TTIP–H_2O	150 °C	0-2 nm, 20 cycles	
$0.5Li_2MnO_3{\cdot}0.5LiNi_{0.375}Mn_{0.375}Co_{0.25}O_2$	Al_2O_3	TMA–H_2O	120 °C	<3 nm, 6 cycles	97
	ZrO_2	$Zr(NMe_2)_4$–H_2O	100°, 150 °C		
	TiO_2	TTIP–H_2O	100°, 150 °C		
	$LiAlO_x$	(LiO^tBu–H_2O) + (TMA–H_2O)	225 °C		
$Li_{1.2}Ni_{0.2}Mn_{0.6}O_2$	Al_2O_3	TMA–H_2O	150 °C	~1 nm, 4 cycles	98
$LiNi_{0.5}Mn_{1.5}O_4^{\#}$	Al_2O_3	TMA–H_2O	N/A	2-cycle $LiAlO_2$ on cathode	62
	$LiAlO_2$	(LiO^tBu–H_2O) + (TMA–H_2O)	225 °C		
V_2O_5	Al_2O_3	TMA–H_2O	25 °C	N/A, 10 cycles	99

Footnote: All cathodes were tested using Li metal as counter electrode, unless otherwise notified. # indicates the cathode was tested using graphite as the counter electrode.

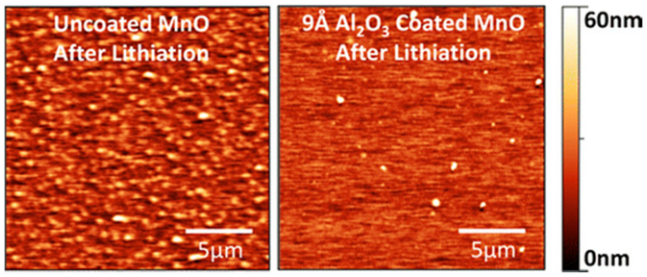

Figure 8. SICM topographical images after lithiation to 0 V for bare MnO (left) and MnO coated with 9 Å of Al_2O_3 (right) [80].—Reprinted with permission from *Chem. Mater.*, **26**, 935 (2014). Copyright 2014, American Chemical Society.

than a single coating (such as Al_2O_3) to improve the overall electrochemical properties of $LiCoO_2$.

ALD surface coatings have also been widely employed in high-voltage cathode materials, including $LiNi_{1/3}Mn_{1/3}Co_{1/3}O_2$ (NMC) [92, 93], $LiNi_{0.5}Mn_{1.5}O_4$ [62, 94], $Li_{1.2}Ni_{0.2}Mn_{0.6}O_2$ [98], $Li_{1.2}Ni_{0.15}Mn_{0.55}Co_{0.1}O_2$ [95], $Li_{1.2}Ni_{0.13}Mn_{0.54}Co_{0.13}O_2$ [96], $Li[Li_{0.20}Mn_{0.54}Ni_{0.13}Co_{0.13}]O_2$ [91], and $0.5Li_2MnO_3{\cdot}0.5LiNi_{0.375}Mn_{0.375}Co_{0.25}O_2$ [97]. These cathode materials are being considered as replacements for $LiCoO_2$ because of their high specific capacity and high working voltage. The high working voltage (4.5–4.8 V *vs* Li^+/Li) can lead to high output energy density of batteries but also can cause serious problems in the cathode and electrolytes. These high-voltage cathode materials suffer from Mn dissolution into the electrolyte through a disproportionation reaction ($2Mn^{3+} \rightarrow Mn^{4+} + Mn^{2+}$) at the cathode surface [93]. Permanent loss of Mn results in the decreased capacity of these cathode materials. Furthermore, Mn^{2+} in the electrolytes tends to migrate to the anode and deposit on the surface of anode materials [62, 94]. The deposition of Mn^{2+} very likely blocks lithium ion transport and damages the SEI film. Ultrathin Al_2O_3 surface coatings by ALD could greatly alleviate the dissolution of Mn, by acting as a physical barrier between cathode and electrolytes. For example, the stability of NMC at an upper cut-off of 4.5 V was greatly enhanced with just a two-cycle Al_2O_3 coating (~0.2 nm thickness) [92]. Capacity retention of NMC was increased from 65% to 91% after 100 cycles at a rate of C/2. Two-cycle Al_2O_3-coated NMC could deliver a discharge capacity of 140 mAh g^{-1} after 100 cycles, in comparison with 103 mAh g^{-1} for pristine NMC. Another study reported that a six-cycle Al_2O_3 coating could improve the capacity retention of a lithium-excess Li $[Li_{0.20}Mn_{0.54}Ni_{0.13}Co_{0.13}]O_2$ cathode [91]. An interesting finding of this work was that the stability could be further enhanced by heat treatment of six-cycle Al_2O_3 coated Li $[Li_{0.20}Mn_{0.54}Ni_{0.13}Co_{0.13}]O_2$ at 300 °C in air for 3 h. The reason was attributed to the formation of a better Li^+ conductive phase (such as layered $Li_{1-x}Al_{1-y}M_yO_2$) at the cathode surface due to inter-diffusion between atoms from the coating and the active material [91]. It should be noted that polytetrafluoroethylene (melting point: ~327 °C), rather than polyvinylidene fluoride, was used as the binder for preparing the electrode [91].

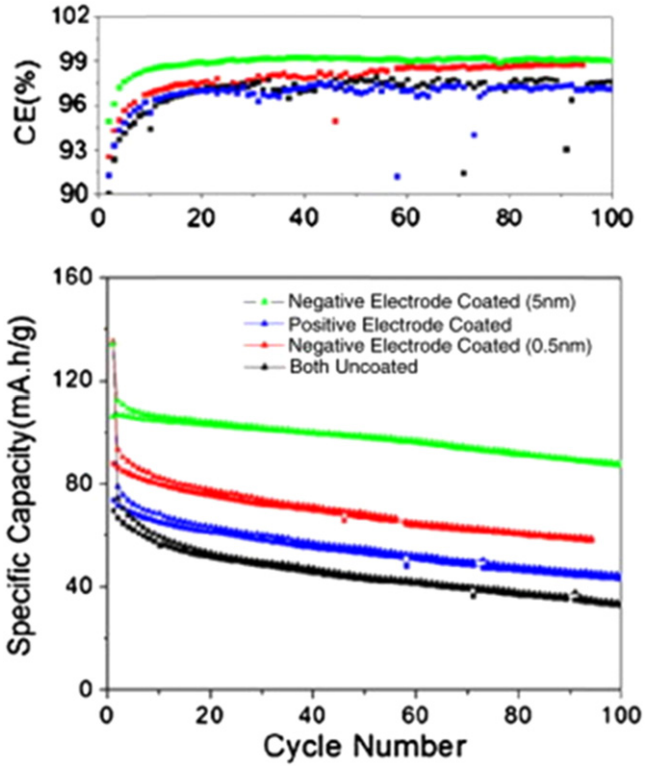

Figure 9. Columbic efficiency and cycling performance of $LiNi_{0.5}Mn_{1.5}O_4$|graphite full cells without Al_2O_3 coating (black), and with Al_2O_3 coating on the negative electrode only (green and red), and positive $LiNi_{0.5}Mn_{1.5}O_4$ only (blue) [94].—Reprinted from *Electrochem. Commun.*, **32**, 31 (2013). Copyright 2013, with permission from Elsevier.

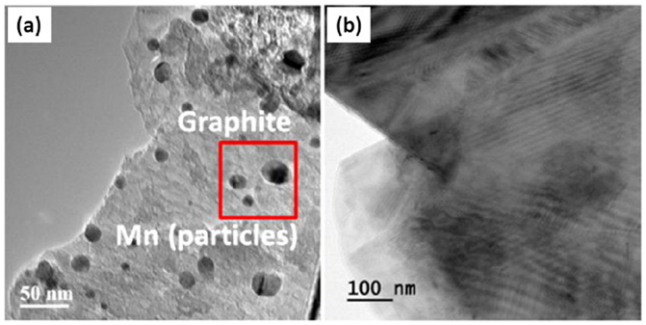

Figure 10. Typical TEM images of graphite anode without (a) and with (b) 0.55 nm Al_2O_3 coating after cycling in $LiNi_{0.5}Mn_{1.5}O_4$| graphite full cells [94]—Reproduced from *Electrochem. Commun.*, **32**, 31 (2013). Copyright 2013, with permission from Elsevier.

The above high-voltage cathode materials were tested in half cells with Li metal as the counter electrode. However, two recent studies [62, 94] have disclosed that when coupled with a graphite anode, the $LiNi_{0.5}Mn_{1.5}O_4$ cathode showed much worse cycling stability, discharge capacity, and columbic efficiency. It is believed that migration of Mn^{2+} and deposition on the graphite was more deleterious for cyclability than Mn loss in $LiNi_{0.5}Mn_{1.5}O_4$ [62, 94]. In this case, ALD Al_2O_3 surface coatings on only the graphite anode were more effective than on only the $LiNi_{0.5}Mn_{1.5}O_4$ cathode or on both electrodes in improving the performance of

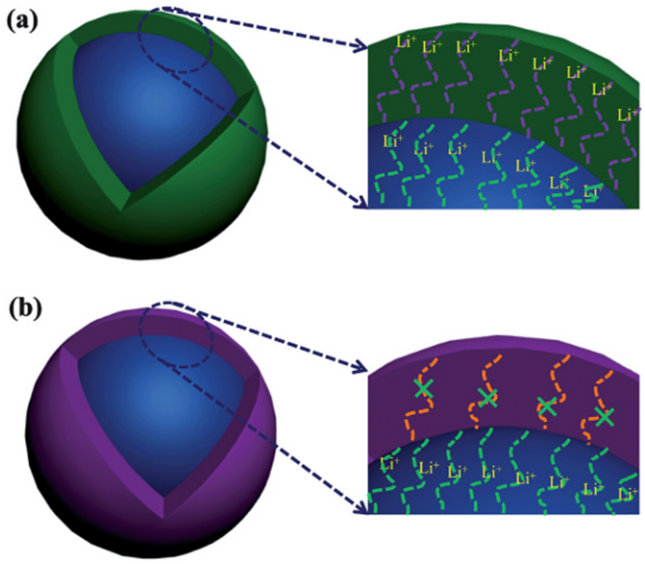

Figure 11. Schematic diagrams of (a) solid-state electrolyte coating and (b) metal oxide coating. The former is expected to provide higher lithium ion conductivity than the latter [93]—Reproduced by permission of The Royal Society of Chemistry.

$LiNi_{0.5}Mn_{1.5}O_4$ in full cells. As seen in figure 9, when only the graphite anode was coated with 5 nm Al_2O_3, $LiNi_{0.5}Mn_{1.5}O_4$ exhibited a discharge capacity of ~90 mAh g^{-1}, which was double than that of uncoated cells and only $LiNi_{0.5}Mn_{1.5}O_4$ coated with Al_2O_3 [94]. A similar trend was also reported by Park *et al* [62], using ALD Al_2O_3 and $LiAlO_2$ surface coatings. Moreover, transmission electron microscopy (TEM) (figure 10) [94] and x-ray absorption near edge structure (XANES) [62] analysis proved that the Mn and/or Ni concentrations on uncoated graphite were dramatically higher than those on only graphite coated with ALD-Al_2O_3. These results suggest it is necessary to use full cells to evaluate the influence of ALD surface coatings on the performance of high-voltage Mn-containing cathode materials.

A new approach to using ALD surface coatings is to develop new coating materials with desirable properties, as described in figure 7. Since metal oxides (such as Al_2O_3 and ZrO_2) are generally poor ionic and electronic conductors, solid-state electrolytes have been proposed as a lithium ion-conducting coating layer to replace metal oxides (figure 11). Proof-of-concept work has been done by using a lithium tantalate solid-state electrolyte prepared by ALD as a coating layer to improve the performance of NMC at high voltages [93]. Lithium tantalate was deposited at 225 °C using an ALD recipe of $(LiO^tBu–H_2O) + 5 \times (Ta(OEt)_5–H_2O)$ and showed an ionic conductivity of 2×10^{-8} S cm^{-1} at RT [50]. Electrochemical testing indicated that the cycling stability and rate capability of NMC was greatly improved with lithium tantalate surface coating, especially at high cutoff voltages up to 4.8 V and a high working temperature (55 °C) [93]. When cycled between 3.0 and 4.8 V, 10-cycle $LiTaO_3$-coated NMC delivered a discharge capacity of 122 mAh g^{-1} after 100 cycles, in comparison with 59 mAh g^{-1} for bare NMC. At 55 °C, NMC coated with five-cycle $LiTaO_3$ showed a discharge capacity of 167 mAh g^{-1} after 100 cycles, corresponding to a 92% capacity retention.

4. Perspectives of future work

4.1. ALD of electrode materials and solid-state electrolytes

A few promising anode materials, such as Si and Sn, haven't been synthesized by ALD for battery application so far. The possibility of using ALD to prepare Si nanoparticles much smaller than their critical breaking size might provide a good solution to the large volume change in Si upon cycling, which is the main reason for the rapid degradation of battery performance [63, 100]. For the cathode, many lithiated materials, including high-voltage cathodes (such as $LiNi_{1/3}Co_{1/3}Mn_{1/3}O_2$ and $LiNi_{1.5}Mn_{0.5}O_4$) and other members of $LiMPO_4$, are to be developed by ALD and tested in 2D or 3D substrates for future all-solid-state microbatteries. Moreover, it is imperative to develop solid-state electrolytes having competitive ionic conductivities with LiPON (figure 6), such as Na super-ionic conductor (NASICON) structured electrolytes ($LiM^{IV}_2(PO_4)_3$, M^{IV} = Ti, Zr, Ge, and Hf) [101].

The subcycle-strategy used for the fabrication of lithiated cathodes and solid-state electrolytes involves complicated surface reactions in each ALD cycle, making it very challenging to develop ALD processes and to control the composition of target materials. Therefore, it is essential to simplify the ALD process for lithium-containing materials. One promising way is to develop double metal alkoxides of lithium precursors, which have desirable element ratios for the target materials [102].

4.2. ALD of surface engineering

From sections 3.1 and 3.2, we can clearly see the effectiveness of ultrathin surface coatings by ALD in improving the performance of both the anode and cathode in LIBs. Then the questions arise, why and how do ultrathin surface coating layers by ALD make such a big difference in the battery performance? Are there better coating materials than the commonly used metal oxides? To answer these questions, therefore, it is imperative to investigate the structural and compositional changes of the ALD surface coating layers before and after cycling.

Let's take the widely used ALD Al_2O_3 coating as an example. Analysis by XANES spectroscopy [77], x-ray photoelectron spectroscopy (XPS) [69, 73], time-of-flight secondary ion mass spectrometry (TOF SIMS) [72, 95], and electron energy loss spectroscopy (EELS) [103] have disclosed that the Al_2O_3 coating layer changes to Li-Al-O glass (with possible AlF_3 and Al_2O_3) during cycling. Li-Al-O glass is an ionic conductor, which can facilitate the transport of lithium ions. This information promoted the use of ALD solid-state electrolytes ($LiTaO_3$ [93] and $LiAlO_2$ [62]) directly as coating layers on the electrode. Moreover, *in situ* TEM observation revealed that the Li-Al-O glass layer remained intact during cycling [103]. The mechanically robust Li-Al-O

glass layer was believed to be a main reason for the improved performance of electrode materials with large volume change (such as Si, Sn, and SnO_2). From the above results, we can see that the properties of ALD surface layers are critical to reaching the optimal performance of electrode materials. A better understanding is still lacking for other ALD coating materials such as ZrO_2 and TiO_2.

One direction of ALD surface coatings is to use new coating materials that have been proven effective in solution-based methods, such as metal phosphates ($AlPO_4$, $TiPO_4$, and $FePO_4$) [9]. $AlPO_4$ has been shown to be superior to metal oxides as a coating layer in cathode materials, due to the strong covalency of PO_4 polyanions with the Al^{3+} in $AlPO_4$ [104]. ALD recipes for metal phosphates have been developed [105–107]. Other types of potential coating materials are ionic and/or electronic conductors, which are expected to prevent unwanted side reactions and at the same time improve diffusion of lithium ions and/or electrons through the coating layers.

At present, the coating materials are mainly inorganic films prepared by ALD. Recently, molecular layer deposition (MLD), an analog to ALD, is emerging as a new technique to achieve uniform and conformal deposition of organic and hybrid organic-inorganic (metalcone) thin films [108, 109]. In a recent study, alucone films prepared by MLD from TMA and glycerol were found to greatly improve the cycling stability, rate capability, and columbic efficiency of Si anodes [110]. It was believed that the alucone coating layer was robust and resilient enough to accommodate the volumetric changes of the Si anode. MLD provides a great variety of organic and hybrid organic-inorganic films [108, 109] that could be adopted as surface coatings for LIBs. Therefore, MLD is expected to play an important role in providing more versatile and effective surface coating materials in the future.

5. Conclusions

ALD has been shown to be a powerful technique for designing a variety of nanostructured electrode materials and solid-state electrolytes as well as depositing ideal surface coating layers on the electrode to improve the battery performance. Great advances have been made in the fabrication of lithium-containing cathode materials and solid-state electrolytes, which are key components for building all-solid-state microbatteries. Due to its exclusive advantages, ALD is an ideal technique to achieve desirable surface coating layers on the electrode of LIBs. The ultrathin surface coatings enabled by ALD can greatly improve the specific capacity, cycling stability, rate capability, and thermal stability of the anode and cathode materials. New coating materials by ALD or MLD have emerged as promising replacements for metal oxides, including solid-state electrolytes, conductive polymer, and hybrid organic-inorganic films. Furthermore, the excellent control over the quality of coating layers and the straightforward coating process promise ALD great potential for industry-level applications in the future.

Acknowledgments

This work was supported by the Nature Sciences and Engineering Research Council of Canada (NSERC), the Canada Research Chair (CRC) Program, the Canada Foundation for Innovation (CFI), the Ontario Research Fund (ORF), and the University of Western Ontario. The authors would like thank Stephen Lawes for polishing the manuscript. Dr Jian Liu is grateful to the Mitacs Elevate Postdoctoral Fellowship Program.

References

[1] Jeong G, Kim Y-U, Kim H, Kim Y-J and Sohn H-J 2011 *Energy Environ. Sci.* **4** 1986
[2] Thackeray M M, Wolverton C and Isaacs E D *Energy Environ. Sci.* **5** 7854
[3] U S Department of Energy 2011 *One Million Electric Vehicles by 2015-February 2011 Status Report, Office of Energy Efficiency and Renewable Energy*
[4] Manthiram A 2011 *J. Phys. Chem. Lett.* **2** 176
[5] Bruce P G, Scrosati B and Tarascon J M 2008 *Angew. Chem. Int. Ed.* **47** 2930
[6] Aricò A S, Bruce P, Scrosati B, Tarascon J-M and Schalkwijk W V 2005 *Nature Mater.* **4** 366
[7] Wu H B, Chen J S, Hng H H and Lou X W 2012 *Nanoscale* **4** 2526
[8] Yuan L-X, Wang Z-H, Zhang W-X, Hu X-L, Chen J-T, Huang Y-H and Goodenough J B 2011 *Energy Environ. Sci.* **4** 269
[9] Li C, Zhang H P, Fu L J, Liu H, Wu Y P, Rahm E, Holze R and Wu H Q 2006 *Electrochim. Acta* **51** 3872
[10] Li H and Zhou H 2012 *Chem. Commun.* **48** 1201
[11] Meng X, Yang X Q and Sun X 2012 *Adv. Mater.* **24** 3589
[12] Knoops H C M, Donders M E, van de Sanden M C M, Notten P H L and Kessels W M M 2012 *J. Vac. Sci. Technol.* A **30** 010801
[13] Nilsen O, Miikkulainen V, Gandrud K B, Østreng E, Ruud A and Fjellvåg H 2014 *Phys. Status Solidi* A **211** 357
[14] Miikkulainen V, Leskelä M, Ritala M and Puurunen R L 2013 *J. Appl. Phys.* **113** 021301
[15] George S M 2010 *Chem. Rev.* **110** 111–31
[16] Pinna N and Knez M 2012 *Atomic Layer Deposition of Nanostructured Materials* (Weinheim: WILEY-VCH)
[17] Elam J W, Routkevitch D, Mardilovich P P and George S M 2003 *Chem. Mater.* **15** 3507
[18] Marichy C, Bechelany M and Pinna N 2012 *Adv. Mater.* **24** 1017
[19] Liu M, Li X, Karuturi S K, Tok A I Y and Fan H J 2012 *Nanoscale* **4** 1522
[20] Bakke J R, Pickrahn K L, Brennan T P and Bent S F 2011 *Nanoscale* **3** 3482
[21] Knez M, Nielsch K and Niinistö L 2007 *Adv. Mater.* **19** 3425
[22] Detavernier C, Dendooven J, Sree S P, Ludwig K F and Martens J A 2011 *Chem. Soc. Rev.* **40** 5242
[23] Xia X, Zeng Z, Li X, Zhang Y, Tu J, Fan N C, Zhang H and Fan H J 2013 *Nanoscale* **5** 6040
[24] Guan C, Zeng Z, Li X, Cao X, Fan Y, Xia X, Pan G, Zhang H and Fan H J 2014 *Small* **2** 300
[25] Donders M E, Oudenhoven J F M, Baggetto L, Knoops H C M, van de Sanden M, Cm M, Kessels W M M and Notten P H L 2010 *ECS Trans.* **33** 213
[26] Oudenhoven J F M, Baggetto L and Notten P H L 2011 *Adv. Energy Mater.* **1** 10
[27] Cheah S K *et al* 2009 *Nano Lett.* **9** 3230

[28] Wang W, Tian M, Abdulagatov A, George S M, Lee Y C and Yang R 2012 *Nano Lett.* **12** 655
[29] Ban C, Xie M, Sun X, Travis J J, Wang G, Sun H, Dillon A C, Lian J and George S M 2013 *Nanotechnology* **24** 424002
[30] Kim S W, Han T H, Kim J, Gwon H, Moon H S, Kang S W, Kim S O and Kang K 2009 *ACS Nano* **3** 1085
[31] Li X *et al* 2012 *Adv. Funct. Mater.* **22** 1647
[32] Aravindan V, Jinesh K B, Prabhakar R R, Kale V S and Madhavi S 2013 *Nano Energy* **2** 720
[33] Donders M E, Knoops H C M, Kessels W M M and Notten P H L 2012 *J. Power Sources* **203** 72
[34] Meng X, Liu J, Li X, Banis M N, Yang J, Li R and Sun X 2013 *RSC Adv.* **3** 7285
[35] Miikkulainen V, Nilsen O, Laitinen M, Sajavaara T and Fjellvåg H 2013 *RSC Adv.* **3** 7537
[36] Meng X, Libera J A, Fister T T, Zhou H, Hedlund J K, Fenter P and Elam J W 2014 *Chem. Mater.* **26** 1029
[37] Meng X *et al* 2014 *Adv. Funct. Mater.* doi:10.1002/adfm.201401002
[38] Chen X, Zhu H, Chen Y-C, Shang Y, Cao A, Hu L and Rubloff G W 2012 *ACS Nano* **6** 7948
[39] Chen X, Pomerantseva E, Banerjee P, Gregorczyk K, Ghodssi R and Rubloff G 2012 *Chem. Mater.* **24** 1255
[40] Østreng E, Gandrud K B, Hu Y, Nilsen O and Fjellvåg H 2014 *J. Mater. Chem.* A **2** 15044
[41] Gandrud K B, Pettersen A, Nilsen O and Fjellvåg H 2013 *J. Mater. Chem.* A **1** 9054
[42] Donders M E, Arnoldbik W M, Knoops H C M, Kessels W M M and Notten P H L 2013 *J. Electrochem. Soc.* **160** A3066
[43] Miikkulainen V, Ruud A, Østreng E, Nilsen O, Laitinen M, Sajavaara T and Fjellvåg H 2014 *J. Phys. Chem.* C **118** 1258
[44] Liu J, Banis M N, Sun Q, Lushington A, Li R, Sham T K and Sun X 2014 *Adv. Mater.* doi:10.1002/adma.201401805
[45] Aaltonen T, Alnes M, Nilsen O, Costelle L and Fjellvåg H 2010 *J. Mater. Chem.* **20** 2877
[46] Aaltonen T, Nilsen O, Magrasó A and Fjellvåg H 2011 *Chem. Mater.* **23** 4669
[47] Comstock D J and Elam J W 2013 *J. Phys. Chem.* C **117** 1677
[48] Hamalainen J, Holopainen J, Munnik F, Hatanpaa T, Heikkila M, Ritala M and Leskela M 2012 *J. Electrochem. Soc.* **159** A259
[49] Hämäläinen J, Munnik F, Hatanpää T, Holopainen J, Ritala M and Leskelä M 2012 *J. Vac. Sci. Technol.* A **30** 01A106
[50] Liu J, Banis M N, Li X, Lushington A, Cai M, Li R, Sham T-K and Sun X 2013 *J. Phys. Chem.* C **117** 20260
[51] Østreng E, Sønsteby H H, Sajavaara T, Nilsen O and Fjellvåg H 2013 *J. Mater. Chem.* C **1** 4283
[52] Østreng E, Vajeeston P, Nilsen O and Fjellvåg H 2012 *RSC Adv.* **2** 6315
[53] Perng Y-C, Cho J, Sun S Y, Membreno D, Cirigliano N, Dunn B and Chang J P 2014 *J. Mater. Chem.* A **2** 9566
[54] Zhu G-N, Wang Y-G and Xia Y-Y 2012 *Energy Environ. Sci.* **5** 6652
[55] Marichy C and Pinna N 2013 *Coord. Chem. Rev.* **257** 3232
[56] Meng X, Geng D, Liu J, Banis M N, Zhang Y, Li R and Sun X 2010 *J. Phys. Chem.* C **114** 18330
[57] Miikkulainen V, Nilsen O, Fjellvåg H, Laitinen M and Sajavaara T 2012 *AVS Int. Conf. on Atomic Layer Deposition* June 17-20) *(Westin Bellevue, Dresden, Germany*
[58] Putkonen M, Aaltonen T, Alnes M, Sajavaara T, Nilsen O and Fjellvåg H 2009 *J. Mater. Chem.* **19** 8767
[59] Dimesso L *et al* 2012 *Chem. Soc. Rev.* **41** 5068
[60] Wang J and Sun X 2012 *Energy Environ. Sci.* **5** 5163
[61] Kamaya N *et al* 2011 *Nature Mater.* **10** 682
[62] Park J S, Meng X, Elam J W, Hao S, Wolverton C, Kim C and Cabana J 2014 *Chem. Mater.* **26** 3128
[63] Wu H and Cui Y 2012 *Nano Today* **7** 414
[64] Chen Z, Qin Y, Amine K and Sun Y K 2010 *J. Mater. Chem.* **20** 7606
[65] Jung Y S, Cavanagh A S, Riley L A, Kang S H, Dillon A C, Groner M D, George S M and Lee S H 2010 *Adv. Mater.* **22** 2172
[66] Lee M-L, Su C-Y, Lin Y-H, Liao S-C, Chen J-M, Perng T-P, Yeh J-W and Shih H C 2013 *J. Power Sources* **244** 410
[67] Wang H-Y and Wang F-M 2013 *J. Power Sources* **233** 1
[68] He Y, Yu X, Wang Y, Li H and Huang X 2011 *Adv. Mater.* **23** 4938
[69] Xiao X, Lu P and Ahn D 2011 *Adv. Mater.* **23** 3911
[70] Kohandehghan A, Kalisvaart P, Cui K, Kupsta M, Memarzadeh E and Mitlin D 2013 *J. Mater. Chem.* A **1** 12850
[71] Lotfabad E M, Kalisvaart P, Cui K, Kohandehghan A, Kupsta M, Olsen B and Mitlin D 2013 *Phys. Chem. Chem. Phys.* **15** 13646
[72] Lotfabad E M, Kalisvaart P, Kohandehghan A, Cui K, Kupsta M, Farbod B and Mitlin D 2014 *J. Mater. Chem.* A **2** 2504
[73] Snyder M Q, Trebukhova S A, Ravdel B, Wheeler M C, DiCarlo J, Tripp C P and DeSisto W J 2007 *J. Power Sources* **165** 379
[74] Liu J, Li X, Cai M, Li R and Sun X 2013 *Electrochim. Acta* **93** 195
[75] Ahn D and Xiao X 2011 *Electrochem. Commun.* **13** 796
[76] Riley L A, Cavanagh A S, George S M, Jung Y S, Yan Y, Lee S H and Dillon A C 2010 *ChemPhysChem* **11** 2124
[77] Wang D, Yang J, Liu J, Li X, Li R, Cai M, Sham T-K and Sun X 2014 *J. Mater. Chem.* A **2** 2306
[78] Lee J-H, Hon M-H, Chung Y-W and Leu I-C 2010 *Appl. Phys.* A **102** 545
[79] Kang E, Jung Y S, Cavanagh A S, Kim G-H, George S M, Dillon A C, Kim J K and Lee J 2011 *Adv. Funct. Mater.* **21** 2430
[80] Lipson A L, Puntambekar K, Comstock D J, Meng X, Geier M L, Elam J W and Hersam M C 2014 *Chem. Mater.* **26** 935
[81] Jung Y S, Cavanagh A S, Dillon A C, Groner M D, George S M and Lee S-H 2010 *J. Electrochem. Soc.* **157** A75
[82] Scott I D, Jung Y S, Cavanagh A S, Yan Y, Dillon A C, George S M and Lee S H 2011 *Nano Lett.* **11** 414
[83] Woo J H, Trevey J E, Cavanagh A S, Choi Y S, Kim S C, George S M, Oh K H and Lee S H 2012 *J. Electrochem. Soc.* **159** A1120
[84] Cheng H-M, Wang F-M, Chu J P, Santhanam R, Rick J and Lo S-C 2012 *J. Phys. Chem.* C **116** 7629
[85] Lee J-T, Wang F-M, Cheng C-S, Li C-C and Lin C-H 2010 *Electrochim. Acta* **55** 4002
[86] Li X, Liu J, Meng X, Tang Y, Banis M N, Yang J, Hu Y, Li R, Cai M and Sun X 2014 *J. Power Sources* **247** 57
[87] Guan D and Wang Y 2012 *Ionics* **19** 1
[88] Guan D, Jeevarajan J A and Wang Y 2011 *Nanoscale* **3** 1465
[89] Zhao J, Qu G, Flake J C and Wang Y 2012 *Chem. Commun.* **48** 8108
[90] Zhao J and Wang Y 2013 *Nano Energy* **2** 882
[91] Seok Jung Y, Cavanagh A S, Yan Y, George S M and Manthiram A 2011 *J. Electrochem. Soc.* **158** A1298
[92] Riley L A, Van Atta S, Cavanagh A S, Yan Y, George S M, Liu P, Dillon A C and Lee S-H 2011 *J. Power Sources* **196** 3317
[93] Li X, Liu J, Banis M N, Lushington A, Li R, Cai M and Sun X 2014 *Energy Environ. Sci.* **7** 768
[94] Xiao X, Ahn D, Liu Z, Kim J-H and Lu P 2013 *Electrochem. Commun.* **32** 31

[95] Bettge M, Li Y, Sankaran B, Rago N D, Spila T, Haasch R T, Petrov I and Abraham D P 2013 *J. Power Sources* **233** 346
[96] Zhang X, Belharouak I, Li L, Lei Y, Elam J W, Nie A, Chen X, Yassar R S and Axelbaum R L 2013 *Adv. Energy Mater.* **3** 1299
[97] Bloom I *et al* 2014 *J. Power Sources* **249** 509
[98] Zhang X, Meng X, Elam J W and Belharouak I 2013 *Solid State Ion.* doi:10.1016/j.ssi.2013.09.052
[99] Liu D, Liu Y, Candelaria S L, Cao G, Liu J and Jeong Y-H 2012 *J. Vac. Sci. Technol.* A **30** 01A123
[100] McDowell M T, Ryu I, Lee S W, Wang C, Nix W D and Cui Y 2012 *Adv. Mater.* **24** 6034
[101] Thangadurai V and Weppner W 2006 *Ionics* **12** 81
[102] Mäntymäki M, Ritala M and Leskelä M 2012 *Coord. Chem. Rev.* **256** 854
[103] Liu Y, Hudak N S, Huber D L, Limmer S J, Sullivan J P and Huang J Y 2011 *Nano Lett.* **11** 4188
[104] Cho J, Kim Y W, Kim B, Lee J G and Park B 2003 *Angew. Chem. Int. Ed.* **42** 1618
[105] Hämäläinen J, Holopainen J, Munnik F, Heikkilä M, Ritala M and Leskelä M 2012 *J. Phys. Chem.* C **116** 5920
[106] Wiedmann M K, Jackson D H K, Pagan-Torres Y J, Cho E, Dumesic J A and Kuech T F 2012 *J. Vac. Sci. Technol.* A **30** 01A134
[107] Liu J, Tang Y, Xiao B, Sham T-K, Li R and Sun X 2013 *RSC Adv.* **3** 4492
[108] Zhou H and Bent S F 2013 *J. Vac. Sci. Technol.* A **31** 040801
[109] Lee B H, Yoon B, Abdulagatov A I, Hall R A and George S M 2013 *Adv. Funct. Mater.* **23** 532
[110] Piper D M, Travis J J, Young M, Son S B, Kim S C, Oh K H, George S M, Ban C and Lee S H 2014 *Adv. Mater.* **26** 1596